# *Real-Time Dynamic Torque and Angular Speed Measuring Device*


Asdrubal Cheng Cen
*Department of Electrical and Computer Engineering*
*University of Alberta*
Edmonton, Canada
chengcen@ualberta.ca

Ethan Maze
*Department of Electrical and Computer Engineering*
*University of Alberta*
Edmonton, Canada
emaze@ualberta.ca

Mohammad Abdullah Hashmi
*Department of Electrical and Computer Engineering*
*University of Alberta*
Edmonton, Canada
hashmi1@ualberta.ca

Vincent Yee
*Department of Electrical and Computer Engineering*
*University of Alberta*
Edmonton, Canada
vyee@ualberta.ca



***Abstract* — Dynamic torque and angular speed measurements of rotating equipment are often essential to determine the condition and performance of most industrial mechanical systems. This capstone project outlines the design and implementation of a compact, durable, yet reliable data acquisition device used to provide the means to measure and report in real-time the torque and speed of a rotating power take-off shaft. A strain-gauge bridge circuit and a hall effect sensor are used to measure torque and speed. An ATMega328P microcontroller captures the output of this data and then streams it continuously to an in-house developed graphical user interface running on the user's computer. The design goals stipulate that the device is to be able to measure torque values up to 2000 ft-lb to within 50 ft-lb of absolute error, and angular speed up to 1500 rpm to within 50 rpm of absolute error. The assembled prototype is considerably compact, sufficiently durable, and reliably operates well within the agreed-upon margins of error, with the torque being reported to be within ±10 ft-lb and speed within ±2 rpm. Based on simulated tests, the device is also theoretically capable to operate under max load conditions of 2000 ft-lb and 1500 rpm without any reduction of measurement accuracy. All the data obtained from the device is graphically visualized in real-time and saved into comma-separated values files as per the requirements.**



***Keywords — Dynamic Torque, Angular Speed, Strain Gauges, Hall-Effect Sensor, Power Takeoff Shaft, Amplification, Filtering, Graphical User Interface***


## I. Introduction

Torque and speed measurements are of great importance to engineers, users, and manufacturers to help determine the condition and performance of most mechanical systems. The ability to have accurate torque and speed measurements enables the capacity to diagnose failures, improve product quality, and maximize the efficiency of the equipment. Therefore, the team has collaborated with Supreme International with the goal of designing and manufacturing a reliable dynamic torque and angular speed data acquisition device that can provide the means to assess and improve the designs of power take-off (PTO) shaft-related equipment. A PTO shaft is a rotating component of a tractor that transfers mechanical power from the engine of a tractor to a component that is towed behind it, which in the case of Supreme International, is a mixer. This measuring device will be inserted between the PTO shaft of a tractor and a mixer via the use of a joint on both sides of the device.

On the surface of the internal measuring shaft, strain gauges connected in a Wheatstone bridge configuration are used to measure any applied torque. The electrical properties of a copper wire stipulate that its resistance is directly proportional to its length. Since a strain gauge becomes elastically deformed upon the application of a load, its resistance varies in proportion to the load applied to it. This characteristic can be utilized to measure the torque of a rotating shaft. The application of torque causes torsional stresses on the shaft which deform the shaft slightly and cause stress on the strain gauge circuits mounted upon it. By supplying a voltage across the strain gauge and measuring its variation, it is possible to obtain the torque applied to the shaft.

The instrument used for the measurement of speed is a hall-effect sensor. The sensor's output is nominally 5V, but in the presence of a strong enough magnetic field, it goes to 0V**.** This property of a hall-effect sensor is utilized by mounting a magnet on the shaft which passes underneath the sensor with every complete revolution of the shaft. This generates a square wave output from the sensor, whose frequency is equal to the angular speed of the shaft in revolutions per second.

Measured data from the instrumentation of the device undergoes extensive processing to attenuate any appended noise due to various factors like temperature, friction, or even low-order harmonics. After the filtered data is captured by the ATMega328P microcontroller (MCU), it is to be streamed over USB universal asynchronous receiver/transmitter (UART) to an in-house developed graphical user interface (GUI) running on the user's computer. This data is visualized in a graphical format in real-time and stored in comma-separated values (CSV) files. This data may then be used by field technicians and the engineering team to improve future designs and assess warranty claims on the equipment.

## II. Implementation

### A. System Block Diagram

A high-level system block diagram of the data acquisition device, which showcases the direct signal paths of both torque and speed signals, is shown in *Figure 1*. A hall effect sensor is utilized to detect the presence of an external magnetic field from a rotating magnet on the shaft. This outputs a square waveform whose frequency can be used to capture the rotational speed of the rotating shaft. Strain gauges in a Wheatstone bridge configuration are used to capture the change in electrical resistance that is applied by the rotating shaft. Processing this electrical signal through low-pass filters, an instrumentation amplifier, as well as an external 24-bit analog-to-digital converter (ADC) allows for a sufficient electrical signal that can be calculated into a reliable torque signal. These two digital signals are captured using an ATMega328P MCU which streams the data using UART via a transistor-transistor logic (TTL) to USB converter to the GUI for storage and visualization.

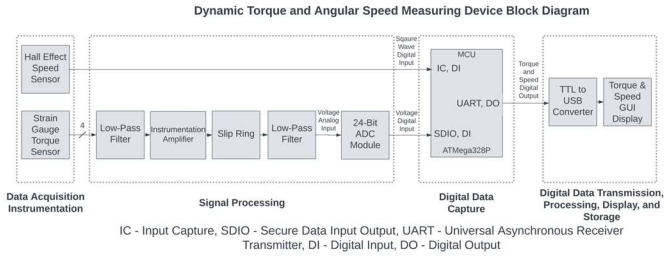


*Figure 1: Block Diagram of the dynamic torque and angular speed measuring device.*

### B. Mechanical Design

The mechanical components of the project are fabricated to create a robust and sturdy platform for the internal electrical components that can handle intense conditions and maintain integrity throughout device operation. The device is a rectangular enclosure created with powder-coated, 3/16" plate steel. The internals of the device are accessible by a hinge on the top of the device with a compression locking latch. Both ends of the enclosure are equipped with a 1 ¾" inner diameter flange-mounted bearing to allow for the measuring shaft to pass into and out of the enclosure. The final assembled enclosure with attached measuring shafts is shown in *Figure 2*.

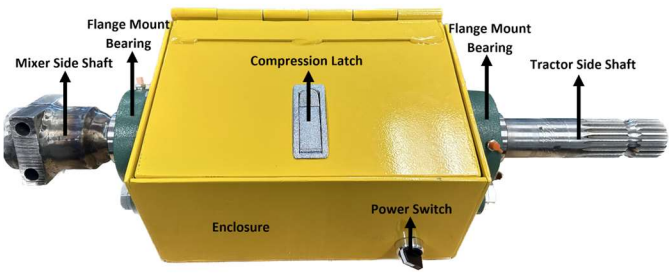


*Figure 2: Final enclosure and shaft design.*

The measuring shaft is a solid 4140 annealed steel shaft to allow the device to withstand the largely applied torque. The shaft of the device itself is 3 separate pieces welded together and machined down to the 1 ¾" outside diameter. The two ends of the device have a female 1 ¾" Z20 spline fitting and a 1 ¾" male fitting to connect to the mixer and tractor PTO shaft respectively. To further support the device and ensure any horizontal forces do not damage the equipment, a bracing device is also designed to be clamped to the frame of the mixer and support the tractor side of the device.

The final dimensions of the enclosure are 11 ⅛" x 7 9/16" x 6" (LxWxH), while the shaft length itself is 28". The weight of the device is 63.8lb, considerably heavier than desired and may be difficult for a single individual to handle. However, the current device is substantially more compact than the existing client device, allowing for greater ease of transportation and storage. The device is still operable by a singular technician and can be maneuvered with proper planning and positioning to ensure the device does not need to be transported over large distances. Furthermore, the substantial decrease in size allows the device to be easily integrated into various platforms without the need for extra equipment or tooling.

The final revision of the device is to include a battery bracket to ensure the battery is secured to the enclosure during operation. Additionally, the main printed circuit board (PCB) board should have mounting holes drilled into the outside of the enclosure to secure the board more permanently and to prevent any possible damage to the board during operation. Such features will be implemented by the client at a future date.

### C. Electrical Design

#### a) Strain Gauges

To accurately and reliably measure a wide range of dynamic torque values, two half-bridge Omega SGT-3FS/350-SY41 strain gauges are installed on the shaft at 180° of separation in a Wheatstone bridge configuration as seen in *Figure 3*.

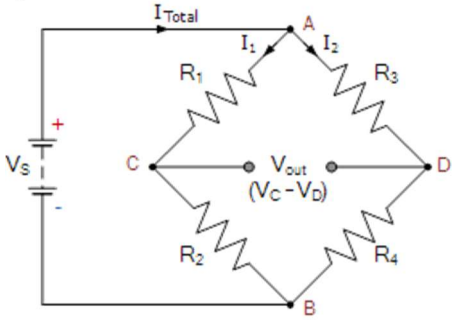


*Figure 3: Wheatstone bridge circuit with 4 strain gauges. [1]*

These gauges have a nominal resistance value of 350Ω under typical conditions when zero torque is applied. This application of the gauges is intended to remove or completely eliminate the effect of axial torque on the gauges and as such only rotational torque will affect the signal [2]. As rotational torque is applied to the shaft, one branch of

the bridge expands while the other contracts resulting in a differential voltage between the positive and negative signal terminals of the bridge. This voltage is processed and calibrated to provide the applied torque on the shaft. Under the assumption of perfect application of the strain gauges, the voltage output is linearly proportional to the torque applied to the shaft. For this device, a voltage of ±5V is applied to the positive and negative terminals respectively which increases the resolution of the signal as the resistance of the branches changes. Given the minuscule resistance changes, the resulting output voltage of the gauges only changes in the 10s of millivolt range. Having a 10V supply differential across the gauges allows for better amplification and signal processing as the signal propagates through the remainder of the components in the system.

*b) Hall-Effect Sensor*

An AH3362Q hall-effect sensor is utilized to provide a non-contact method that is resilient to dust, dirt, and ambient infrared light to measure the angular speed of a rotating shaft. The installed hall-effect sensor has a high switching frequency of 800kHz which allows for the measuring of angular speeds well above the client's stipulated maximum of 1500 rpm. A small cylindrical magnet with an N35 strength is attached to the internal shaft 4mm away from the hall-effect sensor to generate the required magnetic flux. According to (1), this would result in a magnetic flux density of about 30G [3] at the location of the hall effect sensor. Utilizing a Schmitt trigger, the hall-effect sensor outputs a LOW signal when magnetic flux density reaches a threshold of 30G, and outputs a HIGH signal anytime detected flux densities are below this threshold. Anytime the shaft rotates to move the magnet away from the hall-effect sensor, the magnetic flux density rapidly drops below 30G and generates a HIGH voltage output. When the shaft rotates to move the magnet under the hall-effect sensor, the magnetic flux density eventually exceeds 30G and generates a LOW voltage output. This results in a square wave, where each falling edge denotes one complete revolution. The angular speed in revolutions per minute (rpm) is then calculated by taking the reciprocal of the time period in seconds between two falling edges and multiplying it by 60.

$$B = \frac{B_r}{2}\left(\frac{D+z}{\sqrt{(R^2+(D+z)^2)}}\right) - \frac{z}{\sqrt{R^2+z^2}} \quad (1)$$

*c) Slip Ring*

A custom G044-04-53338 slip ring, as seen in *Figure 4*, is integrated into the device to transfer power to the strain gauges and process signals off of the shaft for interpretation. The slip ring is manufactured to accommodate both the tolerance of desired speeds as well as the dimensions of the shaft of the device. The slip ring is IP51 rated with a 4-circuit 5A rated stator/rotor unit with a dynamic noise of less than 0.01Ω. The slip ring is also capable of sustaining temperatures from -30°C to +80°C and speeds between 0 to 2000 rpm in both directions of rotation. Upon independent testing of the slip ring, the noise is seen to be almost negligible. Therefore, with analog and integrated digital filtering, any noise that would be present due to the slip ring is attenuated to an inconsequential amount.

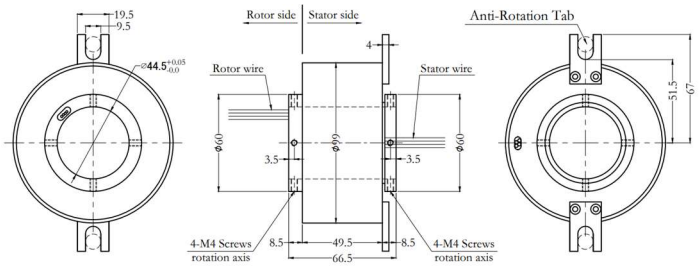


*Figure 4: Slip ring design and specifications.*

*d) Amplification*

The differential voltages outputted from strain gauges are in the millivolt range, which is too insignificant for the ADC to process. As a result, an INA118 instrumentation amplifier as shown in *Figure 5* is incorporated to amplify such differential voltages into an interpretable range. This instrumentation amplifier offers the advantage of reducing the common mode noise ratio, providing high amplification gains, and the low introduction of noise. The amplifier gain is controlled by the resistance of a variable potentiometer with values between 0Ω and 1000Ω calculated using (2).

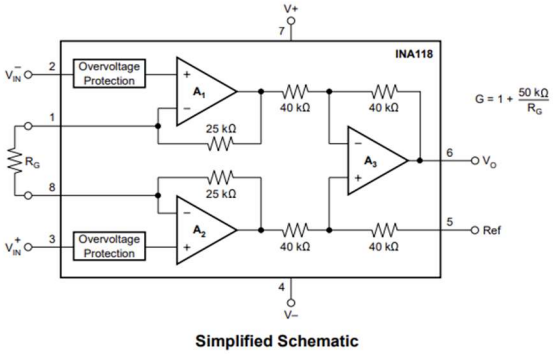


*Figure 5: Internal schematic of the INA118. [4]*

$$\text{Gain} = \frac{50000\ \Omega}{R_g\ (\Omega)} \quad (2)$$

The full Wheatstone bridge outputs an estimated signal of 10mV under 2000 ft-lb with a 10V difference in excitation voltage. A maximum input voltage for the ADC is half of the supplied 5V to power the device, being an input voltage of 2.5V. It is therefore critical to set the amplification gain so as to not amplify the 10mV signal to exceed this maximum 2.5V input voltage as this will result in signal clipping. It is also necessary to not amplify the signal too little so as to result in a reduction of resolution. Therefore, a maximum rated input voltage to the ADC is set to 1.5V at the maximum rated operating load of 2000ft-lb. This is selected to provide ample signal amplification while still leaving room for higher torque operations. Therefore,

the ideal gain is calculated as shown in (3), and the required configured potentiometer resistance is calculated as shown in (4).

$$\text{Gain} = \frac{1.5V}{0.010V} = 150\ V/V \quad (3)$$

$$R_g(\Omega) = \frac{50000\ \Omega}{\text{Gain} - 1} = \frac{50000\ \Omega}{149\ \text{V/V}} = 335\Omega \quad (4)$$

Due to the high sensitivity of the potentiometer, the resistance is set to be 348Ω, which leads to an actual gain of 144.67 V/V.

*e) Filtering*

Various factors like temperature variations in strain gauges, friction introduced by slip rings, voltage spikes created from electromagnetic interferences, or even introduced low-order harmonics from the voltage regulator all play a factor in introducing noise into acquired data. Therefore, an analog, as well as a digital filter are incorporated into the design of the torque-speed sensor device.

The analog implementation phase comprises several simple low-pass filters in a resistor-capacitor configuration, as shown in *Figure 6*. Low-pass filters of capacitive and resistive values of 10uF and 1600Ω respectively are implemented after the load cell and slip ring phases. The corresponding cut-off frequency for this configuration is 9.94Hz.

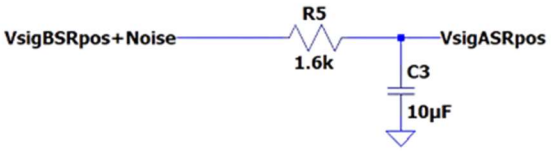


*Figure 6: Analog implementation of the low pass filter.*

As shown in the unfiltered signal in *Figure 7*, noise below 10 Hz along with low-order harmonics introduced from the voltage regulator is being amplified by the instrumentation amplifier, resulting in a still undesirable signal. To further attenuate appended noises, a second-order digital filter is implemented in the GUI. A moving average filter is used [5], where the digital filter takes a window of ten data points received from the MCU and performs a fast Fourier transform to filter out all frequencies except the DC value. An inverse fast Fourier transform is then performed to get the resulting DC value. By repeating the entire procedure twice, a much cleaner torque signal can be obtained as shown in the filtered signal in *Figure 7*. It is found that the signal went from an absolute error of 175 mV to a much more desirable absolute error of less than 25 mV. This digital implementation phase is imperative to achieving a torque signal that is well within the acceptable ±50 ft-lb of torque. *Figure 8* shows the frequency domain of the original signal and the filtered signals. Frequencies past 10Hz are greatly attenuated, resulting in a much less noisy signal being generated. The bumps are due to the window of data points chosen for the filtering process. If a filtering window of 100 points is chosen instead of a 10-point window, the attenuation will be more smooth. Due to the processing time of the algorithm, however, a 10-data point window is selected to achieve as close to real-time data as possible.

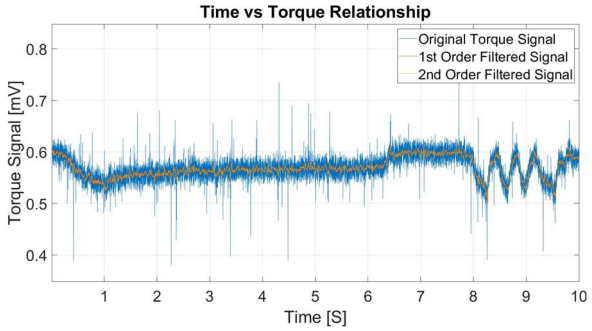


*Figure 7: Torque signal before and after the digital filtering process in the time domain.*

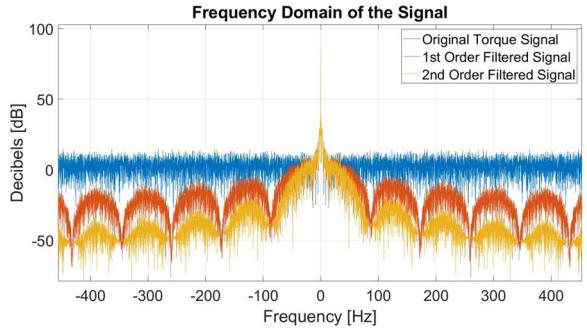


*Figure 8: Torque signal before and after the digital filtering process in the frequency domain. [5]*

*f) Power Circuitry*

Powering the device is a 12V, 7.2Ah rechargeable lead acid battery. This battery is used to power all components that are not directly interfaced with the computer including but not limited to the strain gauge circuitry, amplifiers, switching regulators, the hall-effect sensor, the MCU, and the ADC. This 12V supply is controlled by an isolating switch between the main PCB and the battery, allowing for safe component removal from the boards without causing potential catastrophic shorts while the device is still powered. Upon reaching the main PCB, the 12V passes through a 3.15A fuse and is then regulated down to 5V to supply all the stated components via an LM7805C linear voltage regulator.

A constant voltage supply is necessary to get accurate readings from the strain gauge. Without constant supply voltage, the reading between torque changes will correspondingly not be constant. Through testing, it is seen that the regulator does a great job of maintaining a constant +5V. The maximum rated excitation voltage in between the load cell is 10V. To provide the greatest resolution, an LTC1044 switched capacitor voltage converter is used to generate a -5V supply from the 5V regulator power supply and is applied to the negative supply terminal of the load

cell. Experimentally, the voltage converter did not provide exactly -5V but instead -4.8V. This caused a voltage offset in the load cell of around 600mV after amplification at zero applied torque. This offset is corrected through calibration in the GUI.

## D. Software Design

### a) Firmware

The firmware utilizes a finite-state machine with three states, as shown in *Figure 9*.

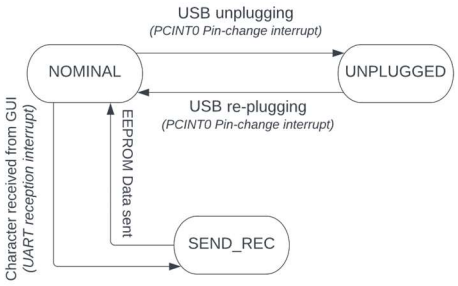


*Figure 9: State machine chart of the firmware.*

#### 1) Nominal State

This is the state where the USB is plugged into the user's computer and the torque and speed data is being streamed to it. The torque data is acquired from an external 24-bit NAU7802 ADC via inter-integrated circuit (I2C) communication, the output of which is a 24-bit signed integer. The speed data is obtained from the hall effect sensor by utilizing the input capture feature of the MCU. The input capture is configured to copy the value inside the timer counter register every time a falling edge is detected. The firmware then calculates the time between two falling edges, taking into account any timer counter overflows that may have occurred as shown in the snippet of code below in *Figure 10*.

```
revs = val - prev_val + 65536 * (num_ovf);
    prev_val = val;
    num_ovf = 0;
```

*Figure 10: Snippet of code used to account for any timer counter overflows.*

Three bytes of torque data and four bytes of speed data are then sent to the GUI using UART through the TTL to USB converter. Before sending the torque value, the character 't' is sent as a sentinel to inform the GUI that the next character is a torque value. Likewise, the character 's' is sent as a sentinel to inform the GUI that the next character is a speed value.

#### 2) Unplugged State

This is the state to which the firmware transitions when the USB is unplugged from the user's computer. The MCU is connected to the PWREN pin of the USB-TTL converter, which uses an active LOW logic. A pin change interrupt is configured on the MCU to enable the transition between the `Nominal` and `Unplugged` states. Once in the `Unplugged` state, the MCU records the torque and speed values every seven seconds and stores them in its EEPROM. A timer interrupt is used to determine precisely when 7 seconds have elapsed. Once the USB is plugged in again, the pin change interrupt detects a LOW logic level and returns the firmware to the `Nominal` state.

#### 3) Send_Rec State

This is a state that is triggered by a UART reception interrupt. When any single character is received from the user over the USB, this interrupt causes a state transition to the `Send_rec` state. When in this state, the data stored in the EEPROM is sent to the user's computer, after which the firmware automatically reverts to the nominal state.

### b) Graphical User Interface (GUI)

The GUI is programmed using the standard GUI library for Python named Tkinter. The GUI enables the user to visualize real-time torque and speed values generated from the rotating PTO shaft and saves the data to desired CSV files. An example GUI with visualized torque and speed values is shown in *Figure 11*.

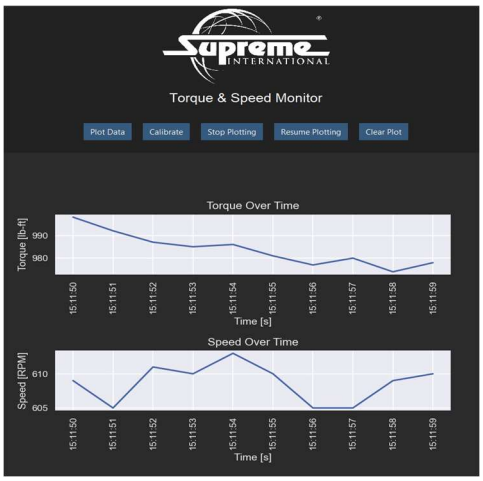


*Figure 11: Graphical user interface design.*

When the torque and speed measurement device is connected to the user's computer via a USB connection, the user has the ability to initiate the plotting of the data via a "Plot Data" button. Upon clicking this button, it initiates the user to select a desired CSV file which data is to be written into. While the data gets updated and displayed in the GUI in real-time, the data will be appended to the selected CSV file in parallel. Due to the nature of the strain gauge application and temperature differentials, the strain gauge's initial mV signal can fluctuate, resulting in a non-zero signal and subsequently a non-zero torque value even with zero applied torque. Therefore, a "Calibrate" button is introduced that can be used prior to operation to offset the initial mV signal down to zero and hence read a zero torque

signal. Other buttons like “Stop Plotting”, “Resume Plotting”, and “Clear Plot” provide greater user capabilities and freedom to manipulate generated data as desired.

## E. *Schematics*

### a) *Mechanical*

The total mechanical design expanded with all components is shown in *Figure 12*.

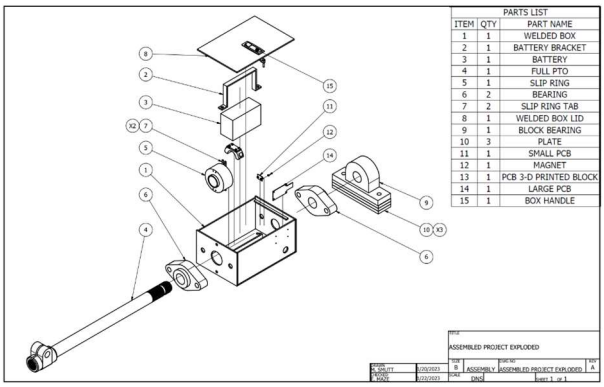


*Figure 12: Exploded mechanical design.*

### b) *Electrical*

The electrical aspect of the torque-speed sensor device comprises three printed circuit boards.

#### 1) *Main-Board*

The main board, as shown in *Figures 13* and *14*, houses the MCU, the ADC, as well as the TTL to USB converter. Its main objective is to process the data from the sensors, transmit such data to the user interface through the UART to TTL converter, and power all the circuitry with a 5V power supply.

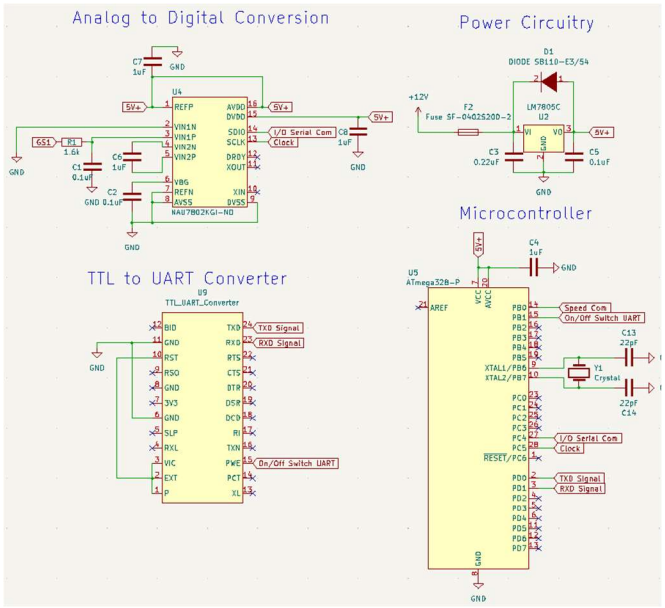


*Figure 13: Schematic of the main board.*

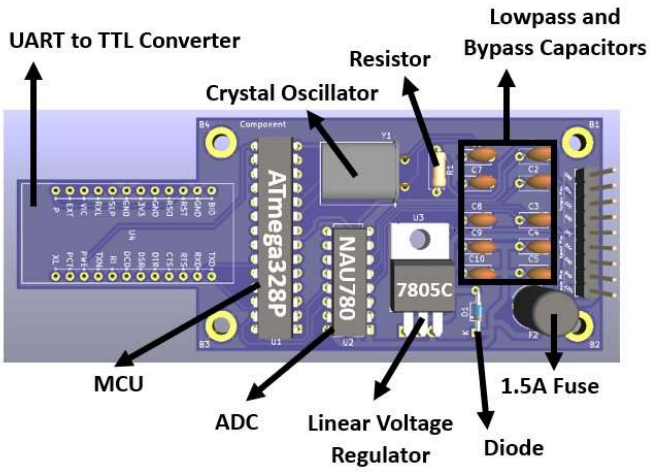


*Figure 14: Printed circuit board of the main board.*

#### 2) *Shaft-Board*

The shaft board, as shown in *Figures 15* and *16*, is mounted on the rotating shaft and houses the low-pass filter and instrumentation amplifier circuitry. Its main objective is to closely filter, amplify and transmit the differential signals from the strain gauges, as well as to provide a negative 5V supply to the load cell for greater resolution.

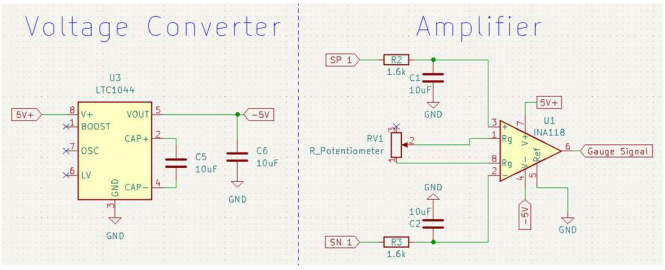


*Figure 15: Schematic of the amplification board.*

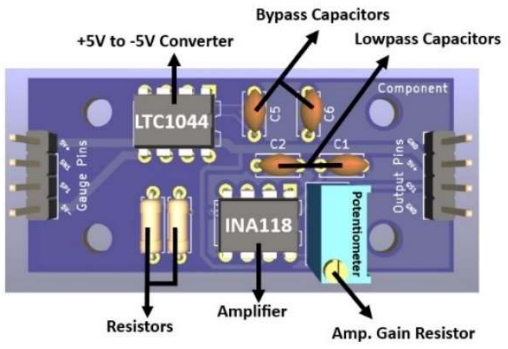


*Figure 16: Printed circuit board of the amplification board.*

#### 3) *Speed-Board*

The speed board, as shown in *Figures 17* and *18*, houses the hall-effect sensor. Its main objective is to place the hall-effect sensor in close proximity to the magnet on

the rotating shaft to detect changes in magnetic fields for angular speed measurements.

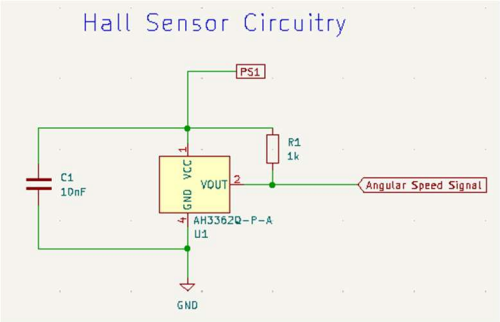


*Figure 17: Schematic of the speed sensor board.*

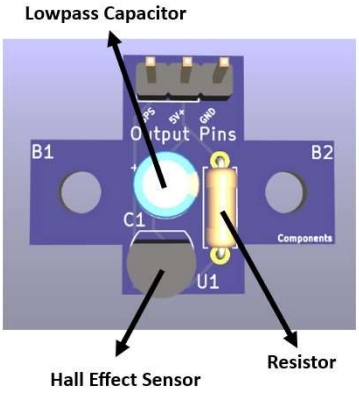


*Figure 18: Printed circuit board of the speed sensor board.*

## III. Results

### A. Calibration

Calibration of device torque is done by clamping one end of the shaft with a swivel vices clamp and applying a known torque to the open-ended shaft through the usage of a torque wrench. As varying torques are applied, the output voltage from the differential amplifier which receives its signals from the strain gauges is monitored and recorded. Temperature variations, misalignments in the application of the gauges, as well as human errors in applying consistent and accurate torque all play a factor in exhibited output voltage. Nonetheless, it is discovered that there is some moderate linearity between applied torque and output differential voltage, as shown in *Figure 19*. Along with torque and differential voltage, additional variations in voltages using the wave generation function of an oscilloscope are done to observe the corresponding relationship of differential voltage and ADC output values. As shown in *Figure 20*, the ADC output to differential voltage is indeed linear. Based on the linearity of ADC output to differential voltage as shown in (5) along with the linearity of differential voltage to torque values as shown in (6), a corresponding linear equation that correlates torque values to ADC outputs is derived as shown in (7).

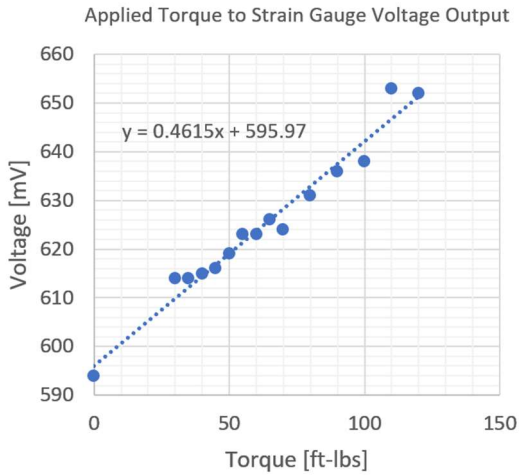


*Figure 19: Differential amplifier output vs applied torque plot.*

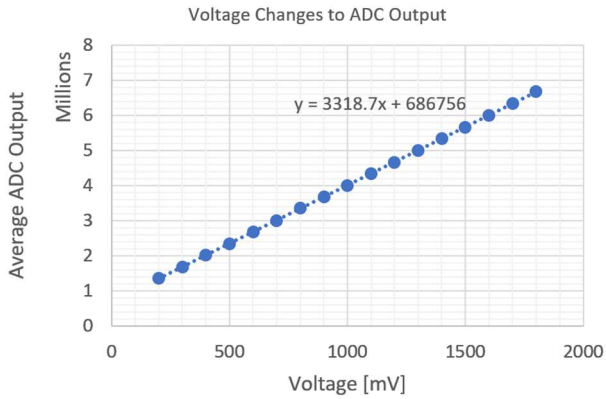


*Figure 20: Analog-to-digital converter output vs differential amplifier input plot.*

$$Voltage = (0.4615 * Torque) + 597.97 \quad (5)$$

$$ADC\ Output = (3318.7 * Voltage) + 686756 \quad (6)$$

$$Torque = (0.00065292 * ADC\ Output) - 1739.773013 \quad (7)$$

Speed values are calibrated using a function signal generator, where input signals are passed through the input capture pin of the MCU. By generating square waveform signals, expected hall-effect sensor outputs can be simulated and used for calibration. By calibrating the device to detect the time between two falling edge pulses of the square waveform, a frequency value can be obtained. By then multiplying this frequency by 60, the angular speed of the rotating shaft in rpm is calculated.

### B. Testing

Using (7), differential voltages that are converted through the ADC are calibrated to an expected torque value. Even with the various negatively impacting factors present, it is found that the resulting calibrated device consistently provided torque readings to within ±10 ft-lb of the expected torque

applied from a torque wrench. This is well within the minimum required accuracy of ±50 ft-lb that is expected from the device.

By using a function signal generator and applying a signal of constant frequency to the input capture pin of the MCU, displayed frequency values in the GUI consistently demonstrated accuracies of up to four decimal places. Multiplying this output frequency by 60 to obtain desired speed values in rpm, therefore, achieves accuracies of less than 1% error, or equivalently accuracy to within ±2 rpm.

Although the device has not been tested in-field to verify its capability to operate under max load conditions of 2000 ft-lb and 1500 rpm, thorough simulated tests have been performed to validate the theoretical capabilities of the data acquisition instrumentation to accurately measure such conditions. By applying a near-maximum differential excitation voltage to the ADC of 2.45V, a torque value of approximately 4015 ft-lb can be detected. Therefore, the desired maximum of 2000 ft-lb of torque is theoretically capable of being detected. Similarly, with generating a constant frequency of 50Hz using a function signal generator, output exhibited frequencies are seen to still be within 4 decimal places. As 50Hz corresponds to 3000 rpm, the device theoretically is able to detect the desired maximum angular speed of 1500 rpm. As enclosure and shaft materials have been specifically chosen, designed, and fabricated to withstand rigorous operating conditions, the device should convincingly be able to operate under desired max load conditions.

## IV. Future Consideration

Some future improvements would be making the enclosure lighter by using a high-strength aluminum alloy, like 7075 aluminum, that is light yet strong enough to withstand the harsh conditions the device will be subject to [6]. Furthermore, the replacement of a lead acid battery with a lithium-ion cell will substantially reduce the size requirement of the enclosure as well. The calibration of the strain gauge could also be made more accurate, in addition, by forming an equation that uses Young's Modulus of the shaft material to correlate the torque value to the voltage output of the strain gauge [7]. Finally, the GUI on the user's side could be improved by the usage of lower latency code, like C++, which improves the data acquisition rate and brings the system closer to real-time.

## V. Conclusion

The fabricated prototype is compact, durable, and able to reliably output speed and torque data to the user's computer, where accuracies of the torque and speed readings are within the margin of error stipulated by the client. The device is also theoretically capable of operating well above the desired maximum load conditions. The acquired data are both displayed in graphical format in real-time and stored on the user's computer through the usage of a developed GUI. Aside from achieving the main project specifications, the device has various additional implemented features that enhance the device's reliability as well as improve the overall user experience. By implementing a feature to calibrate the torque readings before the shaft begins to rotate, the variation of the strain gauge resistance with respect to temperature is considered. Additionally, an error handling routine for instances when the USB comes disconnected from the user's computer is taken into consideration. By a feature where data continues to be collected and stored on the EEPROM of the MCU every 7 seconds for the duration of the USB disconnection, the integrity of torque and speed data is maintained. Overall, the client's requirements are satisfied, and the development of the project is a success.


## Acknowledgement

It is a pleasure to acknowledge the contributions and encouragements of Loren Wyard-Scott, Zoltan Kenwell, Milad Abbasi, as well as Zhaoxiang Zhang. Without their continuous support, the project would likely not have progressed as smoothly or successfully. An additional thanks go to Scott Dewald and Khurram Shah at Supreme International for providing the opportunity to take on this difficult yet exciting project.


## References


[1] W. Storr, "Wheatstone Bridge," Electronics Tutorials, 2014. [Online]. Available: https://www.electronics-tutorials.ws/blog/wheatstone-bridge.html. [Accessed: 05-Apr-2023].

[2] Omega, "Wheatstone Bridge For Strain Gauges," https://www.omega.ca/en/, 04-Nov-2021. [Online]. Available: https://www.omega.ca/en/resources/wheatstone-bridge. [Accessed: 05-Apr-2023].

[3] Supermagnete, "How to Calculate Magnetic Flux Density," Supermangete. [Online]. Available: https://www.supermagnete.de/eng/faq/How-do-you-calculate-the-magnetic-flux-density. [Accessed: 06-Apr-2023].

[4] Texas Instruments, "INA118 Precision, Low-Power Instrumentation Amplifier Datasheet," *Texas Instruments*, Sep-2000. [Online]. Available: https://www.ti.com/lit/ds/symlink/ina118.pdf?HQS=dis-dk-null-digikeymode-dsf-pf-null-wwe&ts=1610500675459. [Accessed: 06-Apr-2023].

[5] G. Hunter, "Windowed Moving Average Filters," mbedded.ninja, 26-Feb-2014. [Online]. Available: https://blog.mbedded.ninja/programming/signal-processing/digital-filters/windowed-moving-average-filters/. [Accessed: 06-Apr-2023].

[6] M. H. Shaeri, M. T. Salehi, S. H. Seyyedein, M. R. Abutalebi, and J. K. Park, "Microstructure and Mechanical Properties of Al-7075 Alloy Processed by Equal Channel Angular Pressing Combined with Aging Treatment," Materials & Design, vol. 57, pp. 250–257, May 2014. [Online]. Available: https://www.sciencedirect.com/science/article/abs/pii/S0261306914000193. [Accessed: 07-Apr-2023].

[7] M. H. Muftah, S. M. Haris, K. Petroczki, and E. A. Khidir, "An Improved Strain Gauge-Based Dynamic Torque Measurement Method," INTERNATIONAL JOURNAL OF CIRCUITS, SYSTEMS AND SIGNAL PROCESSING, vol. 7, no. 1, 2013. [Online]. Available: https://www.naun.org/main/NAUN/circuitssystemssignal/2005-101.pdf. [Accessed: 07-Apr-2023].